

See discussions, stats, and author profiles for this publication at: <https://www.researchgate.net/publication/231647441>

Hydrogen Adsorption on Ga₂O₃ Surface: A Combined Experimental and Computational Study

ARTICLE *in* THE JOURNAL OF PHYSICAL CHEMISTRY C · MAY 2011

Impact Factor: 4.77 · DOI: 10.1021/jp2014226

CITATIONS

17

READS

65

4 AUTHORS, INCLUDING:



Donghai Mei

Pacific Northwest National Laboratory

102 PUBLICATIONS 2,163 CITATIONS

[SEE PROFILE](#)



Chang-Jun Liu

Tianjin University

153 PUBLICATIONS 3,410 CITATIONS

[SEE PROFILE](#)



Qingfeng Ge

Southern Illinois University Carbondale

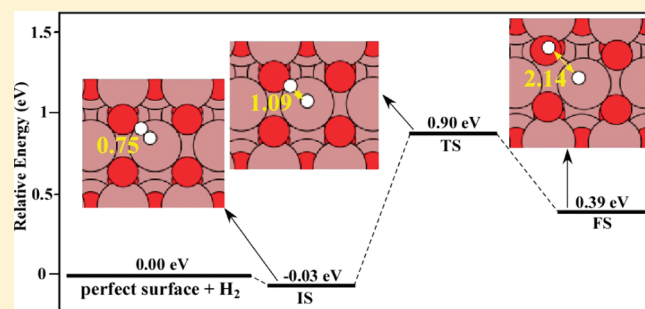
129 PUBLICATIONS 2,733 CITATIONS

[SEE PROFILE](#)

Hydrogen Adsorption on Ga_2O_3 Surface: A Combined Experimental and Computational Study

Yun-xiang Pan,^{†,II} Donghai Mei,[‡] Chang-jun Liu,^{†,*} and Qingfeng Ge^{§,*}[†]Advanced Nano Technology Center, School of Chemical Engineering, Tianjin University, Tianjin 300072, China[‡]Institute for Interfacial Catalysis, Pacific Northwest National Laboratory, Richland, Washington 99352, United States[§]Department of Chemistry and Biochemistry, Southern Illinois University, Carbondale, Illinois 62901, United States

ABSTRACT: In the present work, hydrogen adsorption on the Ga_2O_3 surfaces was investigated using Fourier transform infrared spectroscopy (FTIR) measurements and periodic density functional theory (DFT) calculations. Both the FTIR and DFT studies suggest that H_2 dissociates on the Ga_2O_3 surfaces, producing OH and GaH species. The FTIR bands at 3730, 3700, 3630, and 3600 cm^{-1} are attributed to the vibration of the OH species whereas those at 2070 and 1990 cm^{-1} to the GaH species. The structures of the species detected in experiments are established through a comparison with the DFT calculated stretching frequencies. The O atom of the experimentally detected OH species is believed to originate from the three-coordinated surface O atom. However, the H adatom that binds the coordinately unsaturated Ga atom results in the experimentally detected GaH species. Dissociative adsorption of H_2 on the perfect Ga_2O_3 surface, with the formation of both OH and GaH species, is *endo*thermic and has an energy barrier of 0.90 eV. In contrast, dissociative adsorption of H_2 on the defective Ga_2O_3 surface with oxygen vacancies, which mainly produces GaH species, is *exothermic*, with an energy barrier of 0.61 eV. Accordingly, presence of the oxygen vacancies promotes H_2 dissociation and production of GaH species on the Ga_2O_3 surfaces. Higher temperatures are expected to favor oxygen vacancy creation on the Ga_2O_3 surfaces and thereby benefit the production of GaH species. This analysis is consistent with the FTIR results that the bands assigned to GaH species become stronger at higher temperatures.



1. INTRODUCTION

Gallium oxides have been reported to be a catalyst or cocatalyst for a number of heterogeneous catalytic reactions, which involve the formation and breakage of H-containing bonds,^{1–10} such as water splitting,^{1–3} steam reforming of methane,¹ water gas shift reaction,⁴ reduction of carbon dioxide by methane,^{5,6} and decomposition of volatile aromatic compounds.⁷ In terms of photocatalytic activity, Ga_2O_3 has been shown to have even higher performance than the widely used TiO_2 catalyst.⁷ Key to understanding the mechanism of these reactions is the nature and formation of the H-containing species. Therefore, a detailed characterization of hydrogen adsorption on Ga_2O_3 surfaces will help to identify the catalytically active centers and elucidate the reactivity and selectivity of the catalysts involving Ga_2O_3 . Furthermore, Ga_2O_3 is also outstanding for H₂ detection and used in H₂ sensors.^{11,12} Trinchi et al.¹¹ tested the response of a sensor containing Ga_2O_3 active layers toward different concentrations of H₂ and found that the Ga_2O_3 active layers improved the sensor response to H₂. As such, insight into hydrogen adsorption on Ga_2O_3 surfaces is also crucial for understanding the mechanisms of H₂ detection and further improving the performance of the sensing materials.

There have been several experimental studies focusing on hydrogen adsorption on Ga_2O_3 surfaces.^{4,13–16} Jochum et al.⁴

characterized the H₂ adsorption on Ga_2O_3 surfaces using temperature-programmed desorption and Fourier transform infrared spectroscopy (FTIR) techniques. They found that the adsorption behavior of H₂ is largely dependent upon the substrate temperature. H₂ adsorption on Ga_2O_3 surfaces resulted in OH groups below 200 °C, whereas it only produced GaH species above 200 °C. On the basis of in situ FTIR measurements, Collins et al.¹⁴ proposed that chemisorption of H₂ on Ga_2O_3 surfaces followed two distinct, but complementary, processes: (i) about 27% of H₂ was adsorbed through a homolytic and reversible pathway at 450 °C, forming GaH species; and (ii) the remaining 73% of H₂ dissociated heterolytically on surface Ga—O—Ga sites, producing both GaH and OH species.

A key factor determining the surface chemistry of a metal oxide is the existence of defects such as surface oxygen vacancies.^{15–19} The presence of the oxygen vacancies makes the surface electron-rich, thereby enhancing the electron-donating ability of the surface.¹⁷ Gonzalez et al.¹⁸ found that creation of oxygen vacancies on the $\beta\text{-Ga}_2\text{O}_3(100)$ surface causes the surface to be reactive toward dissociative adsorption of hydrogen.

Received: February 13, 2011

Revised: April 15, 2011

Published: May 03, 2011

Yang et al.¹⁶ reported that the Ga_2O_3 surfaces with oxygen vacancies were more active toward H_2 dissociation. Recently, we showed that the oxygen vacancies are the active centers for the adsorption and activation of CO_2 and the dissociation of H_2O on the Ga_2O_3 surfaces.¹⁸

In the present work, we used a combined experimental and computational approach to study the interaction of H_2 with Ga_2O_3 surfaces. We first characterized the dissociative adsorption of H_2 on Ga_2O_3 surfaces using FTIR measurements. We then used DFT slab calculations to explore the dissociative adsorption of H_2 on a perfect Ga_2O_3 surface and a defective Ga_2O_3 surface with an oxygen vacancy in turn. The results from the experiment and computation are then compared to elucidate the mechanistic origin of the reactivity of Ga_2O_3 toward H_2 dissociative adsorption.

2. EXPERIMENTAL AND COMPUTATIONAL METHODOLOGIES

2.1. Experimental. Ga_2O_3 (purity: 99.999%) used in this work was supplied by Alfa Aesar. Prior to use, it was calcined at 700 °C for 4 h. The FTIR spectra were recorded using a BRUKER Tensor-27 FTIR spectrometer with a resolution of 4 cm^{-1} . During the FTIR study, the sample was held in an IR cell with CaF_2 windows. The sample was heated in a stream of flowing H_2 (30 mL/min) from 25 to 400 °C at a heating rate of 5 °C/min, followed by a stream of flowing helium (30 mL/min) at 400 °C for 30 min. The sample was then cooled down to 25 °C in a stream of flowing helium (30 mL/min). The sample was subsequently heated in a stream of flowing O_2 (30 mL/min) from 25 to 400 °C at a heating rate of 5 °C/min, followed by a stream of flowing helium (30 mL/min) at 400 °C for 30 min. The sample was then cooled down to 50 °C in a stream of flowing helium (30 mL/min). A temperature-programmed reaction was then conducted by heating from 50 to 300 °C (at 5 °C/min) with a H_2 gas flowing at 30 mL/min under the atmospheric pressure.

2.2. Computational. All the calculations were performed in the framework of DFT by using the Vienna ab initio simulation package (VASP).^{20,21} The projector augmented wave method was used to describe the interaction between ions and electrons.^{22,23} The nonlocal exchange-correlation energy was evaluated using the Perdew–Burke–Ernzerhof functional.²⁴ A plane wave basis set with a cutoff energy of 400 eV and a $4 \times 2 \times 1$ k -point grid determined by the Monkhorst–Pack method were found to give converged results. Spin-polarization was included in the calculations involving the defective surface and atomic adsorbates. The atomic structures were relaxed using either the conjugate gradient algorithm or the quasi-Newton scheme as implemented in the VASP code until the forces on all unconstrained atoms were ≤ 0.03 eV/Å.

The $\beta\text{-}\text{Ga}_2\text{O}_3(100)$ surface is the most stable surface and has been used as the substrate in our previous study for CO_2 adsorption and activation.¹⁸ We selected the same slab to represent the $\beta\text{-}\text{Ga}_2\text{O}_3(100)$ surface for hydrogen adsorption in the present study. Briefly, 16 Ga_2O_3 molecular units in the slab were distributed in 6 Ga layers. The vacuum region separating the slabs along the [001] direction was set to 12 Å, resulted in a supercell with a dimension of 6.20 Å \times 11.84 Å \times 22.28 Å. In all calculations, the bottom two layers were frozen in their bulk positions, whereas the top four layers together with the species involved in the dissociative adsorption of hydrogen were allowed to relax.

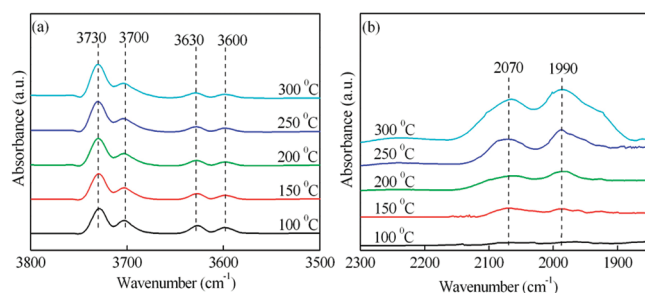


Figure 1. FTIR spectra for hydrogen adsorption on the Ga_2O_3 surfaces in the regions of (a) 3800–3500 cm^{-1} and (b) 2300–1900 cm^{-1} .

Transition states for H_2 dissociation were determined in two steps: first, the nudged elastic band method was used to locate the likely transition states; second, the likely transition states were relaxed using the quasi-Newton algorithm with the same force convergence criterion. Each transition state was confirmed by vibrational frequency analysis. The structure having one and only one imaginary frequency corresponds to a transition state.

3. RESULTS AND DISCUSSION

3.1. FTIR Results. Vibrational spectroscopic methods such as FTIR have been often used to characterize stable adsorption species. Regarding the H_2 adsorption on Ga_2O_3 surfaces, Jochum et al.⁴ observed four distinct FTIR bands at 2025, 2010, 1980, and 1970 cm^{-1} and assigned these bands to different GaH vibrations. The OH region in the FTIR spectrum reported by Jochum et al.⁴ was an uncharacteristic broad and high-intensity band at around 3500 cm^{-1} . Collins et al.¹⁴ also conducted FTIR measurements for H_2 adsorption on Ga_2O_3 surfaces. They found that the bands of the OH group were in the 3800–3000 cm^{-1} region, and the bands at 2003 and 1980 cm^{-1} were assigned to the stretching modes of H bonded to coordinately unsaturated Ga sites.

Figure 1 shows the FTIR spectra measured in our present work. Herein, we focus on two regions of the FTIR spectra: 3800–3500 cm^{-1} and 2300–1900 cm^{-1} . As shown in part a of Figure 1, there are four peaks, that is 3730, 3700, 3630, and 3600 cm^{-1} , in the 3800–3500 cm^{-1} region. These peaks are attributed to the vibration of OH groups on Ga_2O_3 surfaces.^{18,25–27} One possible origin of the OH groups is the dissociative adsorption of H_2 on the surface Ga–O–Ga sites, as suggested by Collins et al.¹⁴ The FTIR spectra in the 2300–1900 cm^{-1} region exhibit bands at 2070 cm^{-1} and 1990 cm^{-1} . These two bands are very close to the FTIR bands for the vibration of GaH species reported by Jochum et al.⁴ and Collins et al.¹⁴ Therefore, we ascribe these two bands to the vibration of GaH species. As shown in part b of Figure 1, the intensity of the bands at 2070 and 1990 cm^{-1} becomes stronger as the temperature increases from 100 to 300 °C. This can be attributed to the increased number of coordinately unsaturated Ga sites at higher temperatures, as proposed by Jochum et al.⁴ In summary, the experimental results indicate that the dissociative adsorption of H_2 on Ga_2O_3 surfaces produces both OH and GaH species.

3.2. DFT Study of H_2 Dissociative Adsorption on $\beta\text{-}\text{Ga}_2\text{O}_3$ –(100) Surfaces. To understand the results obtained from FTIR experiments, we explored the dissociative adsorption of H_2 on the Ga_2O_3 surfaces using the DFT slab calculations. The Ga_2O_3 samples used in the experimental studies have been characterized using the X-ray diffraction (XRD) technique similar to our

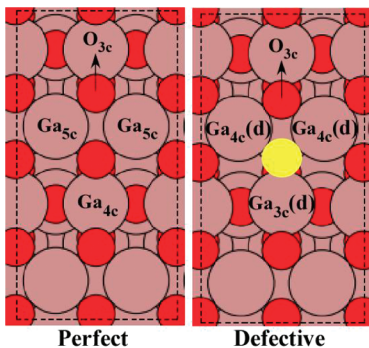


Figure 2. Top views of the perfect $\beta\text{-Ga}_2\text{O}_3(100)$ surface (left panel) and the defective $\beta\text{-Ga}_2\text{O}_3(100)$ surface with an oxygen vacancy (right panel). The oxygen vacancy site was shown as a yellow circle. Color coding: red, O atoms; brown, Ga atoms.

previous work.⁹ The XRD patterns of the Ga_2O_3 sample indicated that the structure is similar to that of $\beta\text{-Ga}_2\text{O}_3$ reported in the literature.^{28–31} In fact, among the five different polymorphs of Ga_2O_3 , that is α , β , γ , δ , and ε , $\beta\text{-Ga}_2\text{O}_3$ is the only stable one under ambient conditions.^{32–34} Heating other forms of Ga_2O_3 or its hydrate will lead to $\beta\text{-Ga}_2\text{O}_3$.³⁵ Moreover, the (100) surface is the most stable and widely studied surface of $\beta\text{-Ga}_2\text{O}_3$ among different surfaces of $\beta\text{-Ga}_2\text{O}_3$.^{15,36} Therefore, we selected the perfect $\beta\text{-Ga}_2\text{O}_3(100)$ surface and defective $\beta\text{-Ga}_2\text{O}_3(100)$ surface with an oxygen vacancy as models in our DFT calculations. For clarity, we use PH to prefix the H adsorption configurations on the perfect surface and DH to prefix those on the defective surface. For example, PH_O_{3c} represents the configuration of the H adatom occupying on the O_{3c} site of the perfect surface whereas DH_Ga_{4c(d)} refers to the configuration of the H adatom on the Ga_{4c(d)} site of the defective surface.

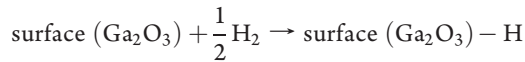
3.2.1. $\beta\text{-Ga}_2\text{O}_3(100)$ Surfaces. The perfect $\beta\text{-Ga}_2\text{O}_3(100)$ surface and defective $\beta\text{-Ga}_2\text{O}_3(100)$ surface with an oxygen vacancy have been analyzed in detail in our previous studies.¹⁸ Figure 2 presents the top views of the two $\beta\text{-Ga}_2\text{O}_3(100)$ surfaces for easy reference. There are 3-fold-coordinated O (O_{3c}), 5-fold-coordinated Ga (Ga_{5c}), and 4-fold-coordinated Ga (Ga_{4c}) sites on the perfect $\beta\text{-Ga}_2\text{O}_3(100)$ surface. The O_{3c} and Ga_{5c} sites are from the 4-fold-coordinated O (O_{4c}) and 6-fold-coordinated Ga (Ga_{6c}) atoms of the bulk $\beta\text{-Ga}_2\text{O}_3$ respectively and are therefore coordinately unsaturated. The Ga_{4c} site is saturated as it is from the Ga_{4c} atom of the bulk $\beta\text{-Ga}_2\text{O}_3$. The defective $\beta\text{-Ga}_2\text{O}_3(100)$ surface with an oxygen vacancy is created by removing a surface O_{3c} atom from the perfect $\beta\text{-Ga}_2\text{O}_3(100)$ surface. The original Ga_{5c} and Ga_{4c} atoms bound to the O_{3c} atom at the vacancy site become four- and three-coordinated, and are denoted as Ga_{4c(d)} and Ga_{3c(d)} respectively as shown in Figure 2. It should be noted that the nature of the Ga_{4c(d)} atom may be different from the Ga_{4c} atoms on the perfect surface. The formation energy of an oxygen vacancy is defined with respect to the gas-phase energy of O₂ in the triplet state, i.e. $E_{V_o} = -(E_{\text{perfect}} - E_{\text{defective}} - \frac{1}{2}E_{\text{O}_2})$. Accordingly, the calculated oxygen vacancy formation energy on $\beta\text{-Ga}_2\text{O}_3(100)$ is 0.34 eV, indicating that the formation of a surface oxygen vacancy on $\beta\text{-Ga}_2\text{O}_3(100)$ is facile.

3.2.2. H Adatom on $\beta\text{-Ga}_2\text{O}_3(100)$ Surfaces. In present study, the formation of a H adatom on the surface was

Table 1. Calculated Structural Parameters (\AA), Vibrational Frequencies (cm^{-1}) and Adsorption Energies (eV) for H Adsorbed on the $\beta\text{-Ga}_2\text{O}_3(100)$ Surfaces

	bond length	vibrational frequency	adsorption energy
PH_O _{3c}	O–H 0.98	$\nu(\text{OH})$ 3644	$\nu(\text{GaH})$ 0.11
PH_Ga _{5c}	1.70	2190	0.51
DH_Ga _{3c(d)}	1.63	2012	-0.29
DH_Ga _{4c(d)}	1.69	2098	-0.18
DH_O _{3c}	0.98	3720	0.03
experiments		3730, 3700, 3630, 3600	2070, 1990

considered as a result of the following dissociative adsorption of hydrogen:



On the basis of this process, the adsorption energy of forming a H adatom, $\Delta E_{\text{ad}}^{\text{H}}$, can be defined as:

$$\Delta E_{\text{ad}}^{\text{H}} = E_{\text{H}/\beta\text{-Ga}_2\text{O}_3} - E_{\beta\text{-Ga}_2\text{O}_3} - \frac{1}{2}E_{\text{H}_2}$$

where $E_{\text{H}/\beta\text{-Ga}_2\text{O}_3}$, $E_{\beta\text{-Ga}_2\text{O}_3}$, and E_{H_2} represent the total energies of the $\beta\text{-Ga}_2\text{O}_3(100)$ slab with an adsorbed H, the clean $\beta\text{-Ga}_2\text{O}_3(100)$ slab and a free H₂ molecule in the vacuum, respectively. E_{H_2} was computed by placing a single H₂ molecule in a $10 \times 10 \times 10 \text{ \AA}^3$ cubic box. According to the definition, a negative value indicates an exothermic or thermodynamically favorable dissociative adsorption. However, a positive value shows the binding strength of the H adatom to the surface is weaker than H–H bond in the gas phase (one-half of the H–H bond energy).

H adatom on the perfect $\beta\text{-Ga}_2\text{O}_3(100)$ surface has two configurations of PH_O_{3c} and PH_Ga_{5c}. The calculated adsorption energies and structural parameters of PH_O_{3c} and PH_Ga_{5c} are given in Table 1. In PH_O_{3c}, the H adatom binds a surface O_{3c} atom, forming an O_{3c}–H bond (0.98 Å). The H-bound O_{3c} atom is pulled out of the surface plane by 0.11 Å. In PH_Ga_{5c}, the H adatom binds to a surface Ga_{5c} atom, with a Ga–H bond length of 1.70 Å. The Ga_{5c} atom is relaxed upward by 0.13 Å. The $\Delta E_{\text{ad}}^{\text{H}}$ of H adatom in PH_O_{3c} and PH_Ga_{5c} are 0.11 and 0.51 eV, respectively. Therefore, on the perfect surface, the H adatom at the O_{3c} site is more favorable than it on the Ga_{5c} site. Figure 3 shows the top view of PH_O_{3c}.

On the defective $\beta\text{-Ga}_2\text{O}_3(100)$ surface with an oxygen vacancy, three possible sites around the oxygen vacancy, that is Ga_{3c(d)}, Ga_{4c(d)}, and O_{3c} sites, are available for the H adatom. This leads to three configurations, that is DH_Ga_{3c(d)}, DH_Ga_{4c(d)}, and DH_O_{3c}. In DH_Ga_{3c(d)}, the H adatom binds the Ga_{3c(d)} atom, with a distance of 1.63 Å. Compared to that on the bare surface, the Ga_{3c(d)} atom is relaxed downward by 0.10 Å due to the H adatom. In DH_Ga_{4c(d)}, the H adatom binds the Ga_{4c(d)} atom, with a distance of 1.69 Å. Consequently, the Ga_{4c(d)} atom is relaxed downward by 0.08 Å. Formation of the O_{3c}–H bond (0.98 Å) in DH_O_{3c} causes the O_{3c} atom to be relaxed upward, by 0.05 Å. The $\Delta E_{\text{ad}}^{\text{H}}$ for the H adatom in DH_Ga_{3c(d)}, DH_Ga_{4c(d)}, and DH_O_{3c} are -0.29, -0.18, and 0.03 eV, respectively. These results indicate that the H

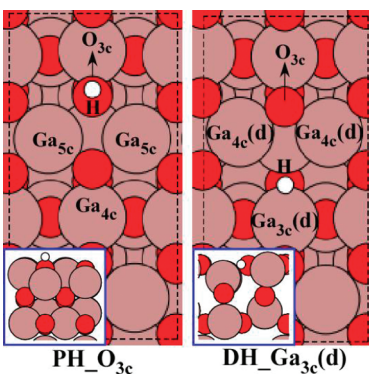


Figure 3. Structures of **PH_O_{3c}** (left panel) and **DH_Ga_{3c}(d)** (right panel). The inset of each panel is the side view. Color coding: white, H atoms; others are the same as in Figure 2.

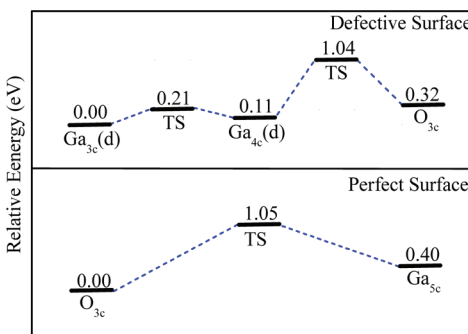


Figure 4. Potential energy profiles for the adsorbed H atom to migrate on the perfect and defective $\beta\text{-Ga}_2\text{O}_3(100)$ surfaces. See Figures 2 and 3 for color coding.

adatom prefers to adsorb at the Ga_{3c}(d) site on the defective surface. Figure 3 illustrates the top view of DH_Ga_{3c}(d).

3.2.3. Diffusion of H Adatom on $\beta\text{-Ga}_2\text{O}_3(100)$ Surfaces. In this section, we will explore the energetics for the H adatom to diffuse on the perfect and defective $\beta\text{-Ga}_2\text{O}_3(100)$ surfaces. Figure 4 shows the potential energy diagrams for H adatom diffusion. On the perfect surface, diffusion of the H adatom from the O_{3c} site to the Ga_{5c} site is endothermic, by 0.40 eV, and has an energy barrier of 1.05 eV. This indicates that diffusion of the H adatom on the perfect surface is difficult, both thermodynamically and kinetically. Therefore, after adsorption on the perfect surface, the H adatom prefers to stay at the O_{3c} site, which is the most favorable adsorption site. On the defective surface, moving the H adatom from the Ga_{3c}(d) site to the Ga_{4c}(d) site is endothermic, by 0.11 eV, with an energy barrier of 0.21 eV, and moving the H adatom from the Ga_{4c}(d) site to the O_{3c} site is endothermic, by 0.21 eV, with an energy barrier of 0.93 eV. Accordingly, similar to that on the perfect surface, the diffusion of the H adatom on the defective surface is also not facile.

3.2.4. Dissociative Adsorption of H₂ on $\beta\text{-Ga}_2\text{O}_3(100)$. The simulated dissociative adsorption process of H₂ on the $\beta\text{-Ga}_2\text{O}_3(100)$ surface, either perfect or defective, proceeds through four different states: (i) bare surface and an isolated H₂ molecule in vacuum; (ii) the molecularly adsorbed H₂ precursor on the surface; (iii) dissociation transition state; and (iv) dissociated adsorption state or product. In the following discussion, state (i) is used as the reference for energetics. The molecularly adsorbed

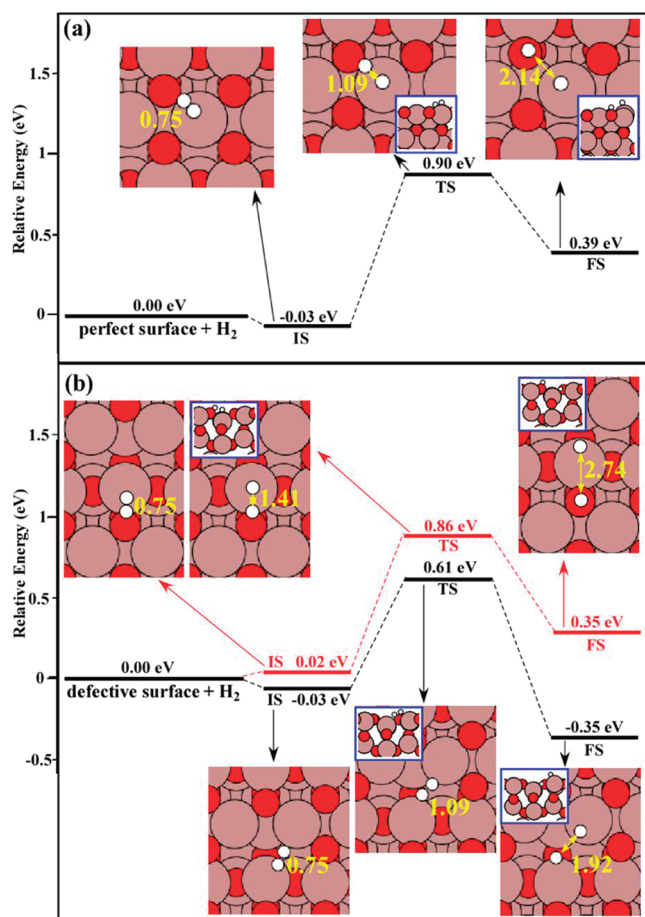


Figure 5. Potential energy profiles for dissociative adsorption of H₂ on (a) perfect and (b) defective $\beta\text{-Ga}_2\text{O}_3(100)$ surfaces. The inset in the blue frame shows the side view of the corresponding structure. The yellow numbers in the inset are the distances in Å. See Figures 2 and 3 for color coding.

H₂, that is state (ii), is the initial state for dissociation. For clarity, the initial, transition and final states are represented by IS, TS, and FS, respectively.

Part a of Figure 5 shows the potential energy diagram for the dissociative adsorption of a H₂ molecule on the perfect $\beta\text{-Ga}_2\text{O}_3(100)$ surface as well as the structures of IS, TS, and FS. As the dissociation progresses, the two H atoms move away from each other. In IS, the H–H bond is 0.75 Å. In TS, the H–H distance is stretched to 1.09 Å. In TS, the O_{3c}–H distance is 1.35 Å and the Ga_{5c}–H distance is 2.14 Å. Finally, the H–H bond is replaced by a new O_{3c}–H bond with a bond length of 0.98 Å and a new Ga_{5c}–H bond with a distance of 1.60 Å in FS. The dissociative adsorption of H₂ on the perfect surface is endothermic, by 0.39 eV, and has an energy barrier of 0.90 eV.

The potential energy diagram for dissociative adsorption of H₂ at the Ga_{3c}(d)–O_{3c} site of the defective $\beta\text{-Ga}_2\text{O}_3(100)$ surface is shown in part b of Figure 5 (red line). Similar to that on the perfect surface, the two H atoms of the molecularly adsorbed H₂ move away from each other as the dissociation progresses. In IS, the H–H bond is 0.75 Å. In TS, the H–H distance is lengthened to 1.41 Å. Finally, in FS, the H–H bond is replaced by a new Ga_{3c}(d)–H bond (1.63 Å) and a new O_{3c}–H bond (0.98 Å). The dissociative adsorption of H₂ at the Ga_{3c}(d)–O_{3c} site is

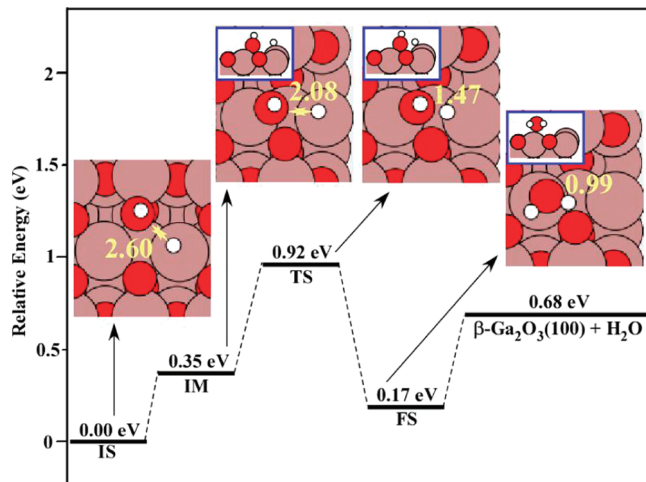


Figure 6. Potential energy profile for water formation on the perfect $\beta\text{-Ga}_2\text{O}_3(100)$ surface after the dissociative adsorption of H_2 across the $\text{Ga}_{3c}-\text{O}_{3c}$ sites. The inset in the blue frame is the side view of the corresponding structure. The yellow numbers in the insets are the distances in Å. See Figures 2 and 3 for color coding.

endothermic, by 0.35 eV, and the energy barrier is 0.86 eV. The black line in part b of Figure 5 presents the potential energy diagram for dissociative adsorption of H_2 over the $\text{Ga}_{3c}(d)-\text{Ga}_{4c}(d)$ site of the defective $\beta\text{-Ga}_2\text{O}_3(100)$ surface. Accompanying the dissociation of the molecularly adsorbed H_2 , the $\text{H}-\text{H}$ distance increases from 0.75 Å in IS, to 1.09 Å in TS, and then to 1.92 Å in FS. Correspondingly, the $\text{Ga}_{3c}(d)-\text{H}$ distance decreases from 3.62 Å in IS, to 2.07 Å in TS, and then to 1.59 Å in FS, and the $\text{Ga}_{4c}(d)-\text{H}$ distance decreases from 3.44 Å in IS, to 1.92 Å in TS, and then to 1.57 Å in FS. The dissociative adsorption of H_2 over the $\text{Ga}_{3c}(d)-\text{Ga}_{4c}(d)$ site is exothermic, by 0.35 eV, with an energy barrier of 0.61 eV. Compared with the dissociative adsorption of H_2 at the $\text{Ga}_{3c}(d)-\text{O}_{3c}$ site, the dissociative adsorption over the $\text{Ga}_{3c}(d)-\text{Ga}_{4c}(d)$ site is more favorable.

3.2.5. Water Formation on the Perfect $\beta\text{-Ga}_2\text{O}_3(100)$ Surfaces. The dissociative adsorption of H_2 on the perfect $\beta\text{-Ga}_2\text{O}_3(100)$ surface produces an O_{3c}H group and a GaH species (part a of Figure 5). The O_{3c}H group and the H adatom of the GaH species can be combined to form a water molecule. Desorption of the water molecule from the perfect surface will create an oxygen vacancy. Figure 6 shows the potential energy diagram for the water formation and desorption process. Similar to that in subsection 3.2.4, the initial, transition, and final states of the process are denoted by IS, TS, and FS, respectively. The process involves an intermediate, represented by IM. The structures of IS, IM, TS, and FS are illustrated in Figure 6.

As shown in Figure 6, the process proceeds in three steps. In the first step, the O_{3c}H group migrates from its original binding site to atop of a Ga_{5c} atom, leading to the conversion from IS to IM. The distance between the O_{3c} atom of the O_{3c}H group and the H atom of the GaH species decreases from 2.60 Å in IS to 2.08 Å in IM. The first step is endothermic, by 0.35 eV. In the second step, the O_{3c}H group in IM binds with the H atom of the GaH species and form a molecularly adsorbed H_2O in FS. The second step has to overcome an energy barrier of 0.57 eV at the transition state TS. In the second step, the distance between the O_{3c} atom of O_{3c}H and the H atom of GaH decreases further,

from 2.08 Å in IM, to 1.47 Å in TS, and finally to 0.99 Å in FS. The product H_2O molecule desorbs from FS in the last step. Desorption of H_2O from the surface needs an energy input of 0.51 eV.

3.3. General Discussion. According to the calculated dissociative adsorption energies (Table 1), the formation of H adatoms on the perfect $\beta\text{-Ga}_2\text{O}_3(100)$ surface from a hydrogen molecule is endothermic, whereas that on the $\text{Ga}_{3c}(d)$ and $\text{Ga}_{4c}(d)$ sites of the defective $\beta\text{-Ga}_2\text{O}_3(100)$ surface with an oxygen vacancy is exothermic. Therefore, the presence of oxygen vacancy promotes the dissociative adsorption of hydrogen. The heterolytic dissociative adsorption of H_2 on the perfect $\beta\text{-Ga}_2\text{O}_3(100)$ surface, with the formation of OH and GaH species, is *endothermic* and has an energy barrier of 0.90 eV. The homolytic dissociative adsorption of H_2 on the defective $\beta\text{-Ga}_2\text{O}_3(100)$ surface with an oxygen vacancy, which produces GaH species, is *exothermic*, with an energy barrier of 0.61 eV. Accordingly, presence of the oxygen vacancies favors the H_2 dissociative adsorption and the production of GaH species. The results are in good agreement with our FTIR experiment that shows the bands assigned to GaH species become stronger at higher temperatures. This can be attributed to the fact that higher temperatures promotes oxygen vacancies creation on Ga_2O_3 surfaces, and thereby enhancing the formation of GaH species, which resulted in stronger GaH bands in the FTIR spectra. The results are also consistent with the results of Gonzalez et al.¹⁵ who reported that creating oxygen vacancies on the $\beta\text{-Ga}_2\text{O}_3(100)$ surface made the surface active toward hydrogen dissociative adsorption.

Next, we correlate the species detected in the FTIR experiments to the computationally determined surface structures. In order to achieve the goal, we performed frequency analysis for configurations of PH-O_{3c} , PH-Ga_{5c} , $\text{DH-Ga}_{3c}(d)$, $\text{DH-Ga}_{4c}(d)$, and DH-O_{3c} . The results are shown in Table 1. The calculated frequencies of the vibration of the OH group, $\nu(\text{OH})$, in PH-O_{3c} and DH-O_{3c} are 3644 and 3720 cm^{-1} , respectively. The calculated $\nu(\text{OH})$ are in good agreement with the experimentally measured values, suggesting that the OH species observed in the experiments are likely in the configurations similar to PH-O_{3c} or DH-O_{3c} . The frequencies of the GaH species, $\nu(\text{GaH})$, in PH-Ga_{5c} , $\text{DH-Ga}_{3c}(d)$, $\text{DH-Ga}_{4c}(d)$ are calculated to be 2190 , 2012 , and 2098 cm^{-1} , respectively. Compared with the calculated $\nu(\text{GaH})$ in PH-Ga_{5c} , the calculated $\nu(\text{GaH})$ in $\text{DH-Ga}_{3c}(d)$ and $\text{DH-Ga}_{4c}(d)$ are closer to the experimentally measured frequencies, as shown in Table 1. As such, the Ga atom of the GaH species detected in the experiments is more likely to be the coordinatively unsaturated Ga atom around the oxygen vacancy, such as the $\text{Ga}_{3c}(d)$ and/or $\text{Ga}_{4c}(d)$ atoms. In addition, these results demonstrate that the surfaces of the Ga_2O_3 sample used in our FTIR experiments are likely defective with oxygen vacancies.

Finally, let us examine the possibility of the H adatom occupying on the Ga_{5c} site. As shown in Figure 5, the H_2 dissociation across the $\text{Ga}_{5c}-\text{O}_{3c}$ site is not facile, both thermodynamically and kinetically. At high temperatures, the dissociation of H_2 across the $\text{Ga}_{5c}-\text{O}_{3c}$ site may take place. However, the H adatom from dissociative adsorption of H_2 will not likely remain at the Ga_{5c} site as the H adatom on the Ga_{5c} site is less favorable than that on the either of the $\text{Ga}_{3c}(d)$, $\text{Ga}_{4c}(d)$, and O_{3c} sites (Table 1). However, the migration of a H adatom from the Ga_{5c} site to the O_{3c} site could be easily achieved at higher temperatures. As shown in Figure 4, diffusion of the H adatom

from Ga_{5c} to O_{3c} is exothermic and has an energy barrier of 0.65 eV. Therefore, the possibility that the H adatom remains at the Ga_{5c} site after the dissociation would be small, even if it was generated as the direct product from H–H bond cleavage at this site. Of course, the possibility is expected to increase as the neighboring favorable sites for H adatoms become occupied.

Whereas there is a qualitative agreement between results from computation and experiment, differences exist at quantitative level. There are many factors that contribute to the differences, for example, the sample used in the experiments is in a powder form whereas the $\beta\text{-Ga}_2\text{O}_3(100)$ surface in perfect and defective form was used in the DFT studies. Although the $\beta\text{-Ga}_2\text{O}_3(100)$ surface may dominate the surface of a powder sample, other types of surface and defects may also contribute to the measured results. Furthermore, our calculated vibrational frequencies are based on harmonic approximation at particular hydrogen coverage, whereas anharmonicity and coverage are expected to affect the measured frequencies and width of the peak. However, the qualitative agreement between the DFT results based on dissociative adsorption of hydrogen on the model Ga_2O_3 surfaces and the results obtained from the FTIR measurements allowed us to establish the structure and nature of the surface hydrogen species. The knowledge will be helpful to understand the activity of catalysts involving Ga_2O_3 and selectivity of processes involving surface hydrogen species.

4. CONCLUSIONS

In the present work, we used FTIR measurements and DFT calculations to study the dissociative adsorption of H_2 on the Ga_2O_3 surfaces. Both the FTIR and DFT studies suggest that the dissociative adsorption of H_2 on the Ga_2O_3 surfaces produces surface OH and GaH species. The FTIR bands at 3730, 3700, 3630, and 3600 cm^{-1} originate from the vibration of the OH species whereas those at 2070 and 1990 cm^{-1} are from the GaH species. The intensity of the bands at 2070 and 1990 cm^{-1} becomes stronger with increasing temperature.

DFT results indicate that dissociative adsorption of hydrogen on the perfect Ga_2O_3 surface was *endothermic*, whereas that on the defective Ga_2O_3 surface with an oxygen vacancy was *exothermic*. Diffusion of the H adatom on the Ga_2O_3 surface, either perfect or defective, is not facile, both thermodynamically and kinetically. Heterolytic H_2 dissociation on the perfect Ga_2O_3 surface, forming coadsorbed OH and GaH species, is *endothermic* and has an energy barrier of 0.90 eV. Homolytic H_2 dissociation on the defective Ga_2O_3 surface with oxygen vacancies, producing only GaH species, is *exothermic* and has an energy barrier of 0.61 eV. Accordingly, the presence of oxygen vacancies on the Ga_2O_3 surfaces promotes H_2 dissociation and production of the GaH species. Higher temperature stabilizes the defective Ga_2O_3 surface with oxygen vacancies and thereby enhances the production of GaH species. This is consistent with the stronger bands associated with the GaH species observed in the FTIR measurements at higher temperatures.

■ AUTHOR INFORMATION

Corresponding Author

*E-mail: ughg_cjl@yahoo.com (C.-j.L.), qge@chem.siu.edu (Q.G.).

Present Addresses

[†]Interdisciplinary Nanoscience Center (iNANO) and Department of Physics and Astronomy, University of Aarhus, 8000 Århus C, Denmark.

■ ACKNOWLEDGMENT

We gratefully acknowledge the support from the National Natural Science Foundation of China (#20990223). D. Mei was supported by a Laboratory Directed Research and Development (LDRD) project at Pacific Northwest National Laboratory (PNNL). The computations were performed using the Molecular Science Computing Facility in the William R. Wiley Environmental Molecular Sciences Laboratory (EMSL), which is a U.S. Department of Energy national scientific user facility located at PNNL in Richland, Washington. Part of the computing time was also granted by the National Energy Research Scientific Computing Center (NERSC) under project No. 752.

■ REFERENCES

- (1) Shimura, K.; Yoshida, T.; Yoshida, H. *J. Phys. Chem. C* **2010**, *114*, 11466.
- (2) Yanagida, T.; Sakata, Y.; Imamura, H. *Chem. Lett.* **2004**, *33*, 726.
- (3) Sakata, Y.; Matsuda, Y.; Yanagida, T.; Hirata, K.; Imamura, H.; Teramura, K. *Catal. Lett.* **2008**, *125*, 22.
- (4) Jochum, W.; Penner, S.; Kramer, R.; Föttinger, K.; Rupprechter, G.; Klötzer, B. *J. Catal.* **2008**, *256*, 278.
- (5) Yuliati, L.; Itoh, H.; Yoshida, H. *Chem. Phys. Lett.* **2008**, *452*, 178.
- (6) Liu, C.-j.; Ye, J.; Jiang, J.; Pan, Y.-x. *ChemCatChem* **2011** in press.
- (7) Hou, Y.; Wu, L.; Wang, X.; Ding, Z.; Li, Z.; Fu, X. *J. Catal.* **2007**, *250*, 12.
- (8) Zhao, B.; Zhang, P. *Powder Technol.* **2010**, *203*, 440.
- (9) Pan, Y.-x.; Kuai, P.; Liu, Y.; Ge, Q.; Liu, C.-j. *Energy Environ. Sci.* **2010**, *3*, 1322.
- (10) Chiavassa, D. L.; Barrandeguy, J.; Bonivardi, A. L.; Baltanas, M. A. *Catal. Today* **2008**, *133*, 780.
- (11) Trinchia, A.; Włodarski, W.; Li, Y. X. *Sens. Actuators, B* **2004**, *100*, 94.
- (12) Weh, T.; Frank, J.; Fleischer, M.; Meixner, H. *Sens. Actuators, B* **2001**, *78*, 202.
- (13) Collins, S. E.; Baltanas, M. A.; Garcia, F. J. L.; Bonivardi, A. L. *J. Catal.* **2002**, *211*, 252.
- (14) Collins, S. E.; Baltanas, M. A.; Bonivardi, A. L. *Langmuir* **2005**, *21*, 962.
- (15) Gonzalez, E. A.; Jasen, P. V.; Juan, A.; Collins, S. E.; Baltanas, M. A.; Bonivardi, A. L. *Surf. Sci.* **2005**, *575*, 171.
- (16) Yang, Y.; Zhang, P. *Phys. Lett., A* **2010**, *374*, 4169.
- (17) Han, Y.; Liu, C.-j.; Ge, Q. *J. Phys. Chem. C* **2007**, *111*, 16397.
- (18) Pan, Y.-x.; Liu, C.-j.; Mei, D.; Ge, Q. *Langmuir* **2010**, *26*, 5551.
- (19) Yamaguchi, K. *Solid State Commun.* **2004**, *131*, 739.
- (20) Kresse, G.; Furthmüller, J. *Phys. Rev., B* **1996**, *54*, 11169.
- (21) Kresse, G.; Hafner, J. *Phys. Rev., B* **1993**, *48*, 13115.
- (22) Blochl, P. E. *Phys. Rev., B* **1994**, *50*, 17953.
- (23) Kresse, G.; Joubert, D. *Phys. Rev., B* **1999**, *59*, 1758.
- (24) Perdew, J. P.; Burke, K.; Ernzerhof, M. *Phys. Rev. Lett.* **1996**, *77*, 3865.
- (25) Digne, M.; Sautet, P.; Raybaud, P.; Euzein, P.; Toulhoat, H. *J. Catal.* **2004**, *226*, 54.
- (26) Digne, M.; Sautet, P.; Raybaud, P.; Euzein, P.; Toulhoat, H. *J. Catal.* **2002**, *211*, 1.
- (27) Pan, Y.-x.; Liu, C.-j.; Ge, Q. *Langmuir* **2008**, *24*, 12410.
- (28) Teramura, K.; Tsuneoka, H.; Shishido, T.; Tanaka, T. *Chem. Phys. Lett.* **2008**, *467*, 191.
- (29) Zheng, B.; Hua, W.; Yue, Y.; Gao, Z. *J. Catal.* **2005**, *232*, 143.
- (30) Hou, Y.; Wang, X.; Wu, L.; Ding, Z.; Fu, X. *Environ. Sci. Technol.* **2006**, *40*, 5799.
- (31) Nishi, K.; Shimizu, K. -i.; Takamatsu, M.; Yoshida, H.; Satsuma, A.; Tanaka, T.; Yoshida, S.; Hattori, T. *J. Phys. Chem. B* **1998**, *102*, 10190.
- (32) Lavallee, J. C.; Daturi, M.; Montouillout, V.; Clet, G.; Arean, C. O.; Delgado, M. R.; Sahibed-dine, A. *Phys. Chem. Chem. Phys.* **2003**, *5*, 1301.

- (33) Vimont, A.; Lavalley, J. C.; Sahibed-Dine, A.; Arean, C. O.; Delgado, M. R.; Daturi, M. *J. Phys. Chem. B* **2005**, *109*, 9656.
- (34) Arean, C. O.; Bellan, A. L.; Mentruit, M. P.; Delgado, M. R.; Palomino, G. T. *Microporous Mesoporous Mater.* **2000**, *40*, 35.
- (35) Roy, R.; Hill, V. G.; Osborn, E. F. *J. Am. Chem. Soc.* **1952**, *74*, 719.
- (36) Bermudez, V. M. *Chem. Phys.* **2006**, *323*, 193.